ITP-SB-94-06

Invariant mass distributions for heavy quark-antiquark pairs in deep inelastic electroproduction

B. W. Harris and J. Smith

Institute for Theoretical Physics,
State University of New York at Stony Brook,
Stony Brook, NY 11794-3840, USA

January 1995

Submitted to Physics Letters B

Abstract

We have completed the $\mathcal{O}(\alpha_s)$ QCD corrections to exclusive heavy quark-antiquark distributions in deep inelastic electroproduction and present here the differential distributions in the masses of charm-anticharm and bottom-antibottom pairs at the electron-proton collider HERA.

Order α_s QCD corrections to the structure functions for single particle inclusive deep inelastic electro-production of heavy quarks were recently published in [1]. The reaction $e^-(l_1) + P(p) \to e^-(l_2) + Q(p_1) + \bar{Q}(p_2) + X$ is dominated by the virtual photon mediated reaction when $-q^2 = -(l_1 - l_2)^2 \ll M_Z^2$, and the heavy quark differential production cross section can be written as

$$\frac{d^2\sigma}{dxdy} = \frac{2\pi\alpha^2}{Q^4} S[\{1 + (1-y)^2\} F_2(x, Q^2, m^2) - y^2 F_L(x, Q^2, m^2)] \,, \tag{1}$$

after integration over the azimuthal angle between the plane containing the incoming and outgoing electron and the plane containing the incoming proton and outgoing heavy quark. The square of the center of momentum energy of the electron-proton system is denoted by S, and the variables x and y are defined as $x = Q^2/2p \cdot q$ and $y = p \cdot q/p \cdot l_1$ with $-q^2 = Q^2 = xyS$. The heavy quark structure functions $F_2(x, Q^2, m^2)$ and $F_L(x, Q^2, m^2)$ are functions of the heavy quark mass m. We assume that the heavy quark production is extrinsic so that F_2 and F_L can be calculated from an analysis of the virtual photon induced reaction $\gamma^*(q) + P(p) \to Q(p_1) + \bar{Q}(p_2) + X$ and its corresponding parton analogue $\gamma^*(q) + a_1(k_1) \to Q(p_1) + \bar{Q}(p_2) + a_2(k_2)$, where a_1 and a_2 are zero-mass gluons g or light mass (anti) quarks $(\bar{q})\, q$ as opposed to the massive (anti) quarks $(\bar{Q})\, Q$. The result is that the structure functions can be obtained from the partonic results via the formula

$$\begin{aligned} F_k(x, Q^2, m^2) &= \frac{Q^2 \alpha_s(\mu^2)}{4\pi^2 m^2} \int_{\xi_{\min}}^1 \frac{d\xi}{\xi} \Big[\, e_H^2 f_g(\xi, \mu^2) c_{k,g}^{(0)} \Big] \\ &+ \frac{Q^2 \alpha_s^2(\mu^2)}{\pi m^2} \int_{\xi_{\min}}^1 \frac{d\xi}{\xi} \Bigg\{ e_H^2 f_g(\xi, \mu^2) \left(c_{k,g}^{(1)} + \bar{c}_{k,g}^{(1)} \ln \frac{\mu^2}{m^2} \right) \\ &+ \sum_{i=q,\bar{q}} f_i(\xi, \mu^2) \left[e_H^2 \left(c_{k,i}^{(1)} + \bar{c}_{k,i}^{(1)} \ln \frac{\mu^2}{m^2} \right) + e_i^2\, d_{k,i}^{(1)} + e_i\, e_H\, o_{k,i}^{(1)} \right] \Bigg\} \,, \end{aligned} \tag{2}$$

where $(k = 2, L)$. The lower boundary on the integration is given by $\xi_{\min} = x(4m^2 + Q^2)/Q^2$. Further $f_i(\xi, \mu^2)\,, (i = g, q, \bar{q})$ denote the parton momentum distributions in the proton, and μ stands for the mass factorization scale which has been put equal to the renormalization scale in the running coupling constant. Finally, $c_{k,i}^{(l)}$ and $\bar{c}_{k,i}^{(1)}\,, (i = g\,, q\,, \bar{q}\,; l = 0, 1)$, and $d_{k,i}^{(1)}$ and $o_{k,i}^{(1)}$, $(i = q\,, \bar{q})$ are scale independent parton coefficient functions which were first calculated in [1]. In Eq. (2) we made a distinction between the coefficient functions with respect to their origin. The coefficient functions indicated by $c_{k,i}^{(l)}$ and $\bar{c}_{k,i}^{(1)}$ originate from the partonic subprocesses where the virtual photon is coupled to the heavy quark hence the factor of e_H^2. The quantity $d_{k,i}^{(1)}$ comes from the subprocess where the virtual photon interacts with the light quark so it is proportional to e_i^2. The quantity $o_{k,i}^{(1)}$ comes from the interference between the above processes and hence has a factor $e_H e_i$ with all charges in units of e. Note that terms proportional to $e_H e_i$ appear in the photon-parton differential distributions even though they integrate to zero in the total partonic cross section. Furthermore we have isolated the

factorization scale dependent term containing $\ln(\mu^2/m^2)$. The functions multiplied by this term, which are indicated by a bar, are called mass factorization parts. Note than Eq. (2) only holds for $Q^2 > 0$. In the photo-production limit there are additional terms involving the parton densities in the photon.

The previous treatment of the $\mathcal{O}(\alpha_s)$ corrections yielded results for the inclusive distributions for heavy quarks in the virtual photon induced reaction $\gamma^* + P(p) \to Q(p_1)(\bar{Q}(p_2)) + X$, i.e., the differentials $dF_k(x, Q^2, m^2, p_t)/dp_t$ and $dF_k(x, Q^2, m^2, y)/dy$. The corrections to the heavy quark inclusive p_t and y distributions at fixed points in Q^2 and x were published in [2]. Event rates for regions of the x and Q^2 plane have been presented in [3].

In this paper we report on the results of a calculation of the $\mathcal{O}(\alpha_s)$ corrections for heavy quark *exclusive* distributions at fixed Q^2 and x, which allows us to study all correlations between the outgoing particles in the virtual photon initiated reaction $\gamma^*(q) + P(p) \to Q(p_1) + \overline{Q}(p_2) + X(k_2)$ with $X = 0$ or 1 jet (massless parton). This information is of immediate interest to the experimenters working with the H1 and ZEUS collaborations at the electron-proton collider HERA. We therefore present the effects of the QCD corrections to invariant mass distributions of a heavy quark-antiquark pair, for $8.5(\mathrm{GeV/c})^2 \leq Q^2 \leq 50(\mathrm{GeV/c})^2$ and $4.2 \times 10^{-4} \leq x \leq 2.7 \times 10^{-3}$. The $(L, 2)$ photon components are treated separately. As input we use the latest CTEQ parton densities [4], which fit the newly released HERA data [5].

Our new analysis of exclusive heavy quark deep inelastic electro-production at HERA extends the existing studies of inclusive QCD corrections in the virtual photon channel [1], [2], [3], inclusive QCD corrections in the real photon ($q^2 = 0$) channel [6], [7], and exclusive QCD corrections in the real photon channel [8], allowing for an extensive comparison with present and future experimental data. Heavy quark electro-production is expected to play an important role in the determination of the gluon distribution function in the proton at small x. A knowledge of the production cross sections and distributions for charm and bottom quarks is also relevant in the study of the CKM matrix elements through the rare decays of $D-$ and $B-$ mesons and the analysis of $D\overline{D}$ and $B\overline{B}$ mixing [9].

In our exclusive computation we use the same techniques as the authors of [8] for computing heavy-quark correlations in photo-production and hadro-production. These are based on the replacement of divergent terms in the squared matrix elements by generalized plus distributions. The divergent terms appear when the propagators diverge in regions of phase space where the outgoing parton is soft and/or collinear to the propagating particle. The replacement of the divergent terms by generalized plus distributions allows one to isolate the soft and collinear poles within the framework of dimensional regularization, without having to calculate all the phase space integrals in a spacetime dimension $n \neq 4$ as usually required in a traditional inclusive computation. The resulting expressions for the squared matrix elements appear in a factorized form where poles in $n-4$ multiply splitting functions and lower order squared matrix elements. The cancelation of singularities is then performed using the factorization theorem [10]. Since the final result is in four-dimensional space time, we can compute all relevant phase space integrations using standard Monte Carlo integration techniques and produce histograms for exclusive, semi-inclusive, or inclusive quantities

related to any of the outgoing particles. We therefore have a new calculation of the scale independent coefficient functions $c^{(l)}_{k,i}$, $\bar{c}^{(1)}_{k,i}$, $d^{(1)}_{k,i}$ and $o^{(1)}_{k,i}$. We checked the $\eta = s/4m^2 - 1$ and $\xi = Q^2/m^2$ dependence of the scale independent coefficient functions against the results in [1]. The analogous results for the inclusive distributions, dF_k/dp_t and dF_k/dy, were also checked against the results in [2]. Additional distributions and correlations along with details of the calculation will be presented in a more complete article [11].

Folding the parton densities in the proton with our new scale independent coefficient functions as dictated by Eq. (2), we present results for the differential structure functions in the invariant mass of the heavy quark-antiquark pair, which we will call M. Thus we give plots of $dF_2(x, Q^2, m^2, M)/dM$ and $dF_L(x, Q^2, m^2, M)/dM$ at fixed x and Q^2. We use $m = m_c = 1.5\,\mathrm{GeV/c^2}$ for charm production and $m = m_b = 4.75\,\mathrm{GeV/c^2}$ for bottom production. We choose the factorization (renormalization) scale as $\mu^2 = Q^2 + 4(m_c^2 + (P_{t_c} + P_{t_{\bar{c}}})^2/4)$ for charm production and $\mu^2 = Q^2 + m_b^2 + (P_{t_b} + P_{t_{\bar{b}}})^2/4$ for bottom production. As mentioned earlier we use the CTEQ3M parton densities [4] in the $\overline{\mathrm{MS}}$ scheme and the two loop α_s with $\Lambda_4 = 0.239\,\mathrm{GeV}$ for charm and $\Lambda_5 = 0.158\,\mathrm{GeV}$ for bottom.

Tables 1 and 2 show the variation of $F_2(x, Q^2, m^2)$ and $F_L(x, Q^2, m^2)$ with the renormalization scale for charm production, and Tables 3 and 4 show the variation for bottom production. For charm production typical variations from the central value are less than 15% and for bottom production they are less than 6%.

Figures 1 and 2 show the distributions $dF_2(x, Q^2, m_c^2, M)/dM$ and $dF_L(x, Q^2, m_c^2, M)/dM$ for charm production at $x = 8.5 \times 10^{-4}$ while varying Q^2. Figure 3 and 4 shows the distributions $dF_2(x, Q^2, m_c^2, M)/dM$ and $dF_L(x, Q^2, m_c^2, M)/dM$ for various values of x at $Q^2 = 12\,(\mathrm{GeV/c})^2$. For charm production, the Born result multiplied by a constant factor gives good agreement with the complete $\mathcal{O}(\alpha_s^2)$ result for the 2 projection, while the L projection is not well reproduced for a constant multiplicative factor for large invariant masses. Figures 5 and 6 show the distributions $dF_2(x, Q^2, m_b^2, M)/dM$ and $dF_L(x, Q^2, m_b^2, M)/dM$ for bottom production at $x = 8.5 \times 10^{-4}$ while varying Q^2. Figure 7 and 8 shows the distributions $dF_2(x, Q^2, m_b^2, M)/dM$ and $dF_L(x, Q^2, m_b^2, M)/dM$ for bottom production for various values of x at $Q^2 = 12\,(\mathrm{GeV/c})^2$. For bottom production, the Born result multiplied by a constant factor gives quite good agreement with the complete $\mathcal{O}(\alpha_s^2)$ result for both the 2 and L projections.

To conclude, we repeat that the invariant mass distributions are reasonably well represented by taking the Born result times a multiplicative factor. The agreement is excellent for bottom production and not quite so good for charm production.

Acknowledgments

We thank J. Whitmore for useful discussions and acknowledge S. Mendoza for help in the early stages of the project. Our research is supported in part by the contract NSF 9309888.

Table 1

x	Q^2	$\mu = \mu_0/2$	$\mu = \mu_0$	$\mu = 2\mu_0$
8.5×10^{-4}	8.5	7.36×10^{-2}	8.43×10^{-2}	9.12×10^{-2}
8.5×10^{-4}	12	0.97×10^{-1}	1.10×10^{-1}	1.20×10^{-1}
8.5×10^{-4}	25	1.57×10^{-1}	1.79×10^{-1}	1.94×10^{-1}
8.5×10^{-4}	50	2.25×10^{-1}	2.52×10^{-1}	2.71×10^{-1}
4.2×10^{-4}	12	1.16×10^{-1}	1.38×10^{-1}	1.54×10^{-1}
8.5×10^{-4}	12	0.97×10^{-1}	1.10×10^{-1}	1.20×10^{-1}
1.6×10^{-3}	12	8.03×10^{-2}	8.89×10^{-2}	9.38×10^{-2}
2.7×10^{-3}	12	6.81×10^{-2}	7.29×10^{-2}	7.48×10^{-2}

Table 1. Variation of F_2 with $\mu_0^2 = Q^2 + 4(m_c^2 + (P_{t_c} + P_{t_{\bar{c}}})^2/4)$ for various x and Q^2 values.

Table 2

x	Q^2	$\mu = \mu_0/2$	$\mu = \mu_0$	$\mu = 2\mu_0$
8.5×10^{-4}	8.5	1.11×10^{-2}	1.23×10^{-2}	1.31×10^{-2}
8.5×10^{-4}	12	1.68×10^{-2}	1.86×10^{-2}	1.99×10^{-2}
8.5×10^{-4}	25	3.32×10^{-2}	3.64×10^{-2}	3.90×10^{-2}
8.5×10^{-4}	50	5.07×10^{-2}	5.51×10^{-2}	5.86×10^{-2}
4.2×10^{-4}	12	2.03×10^{-2}	2.33×10^{-2}	2.55×10^{-2}
8.5×10^{-4}	12	1.68×10^{-2}	1.86×10^{-2}	1.99×10^{-2}
1.6×10^{-3}	12	1.40×10^{-2}	1.50×10^{-2}	1.56×10^{-2}
2.7×10^{-3}	12	1.18×10^{-2}	1.24×10^{-2}	1.26×10^{-2}

Table 2. Variation of F_L with $\mu_0^2 = Q^2 + 4(m_c^2 + (P_{t_c} + P_{t_{\bar{c}}})^2/4)$ for various x and Q^2 values.

Table 3

x	Q^2	$\mu = \mu_0/2$	$\mu = \mu_0$	$\mu = 2\mu_0$
8.5×10^{-4}	8.5	1.53×10^{-3}	1.51×10^{-3}	1.47×10^{-3}
8.5×10^{-4}	12	2.45×10^{-3}	2.45×10^{-3}	2.42×10^{-3}
8.5×10^{-4}	25	6.28×10^{-3}	6.34×10^{-3}	6.36×10^{-3}
8.5×10^{-4}	50	1.37×10^{-2}	1.40×10^{-2}	1.41×10^{-2}
4.2×10^{-4}	12	3.37×10^{-3}	3.44×10^{-3}	3.47×10^{-3}
8.5×10^{-4}	12	2.45×10^{-3}	2.45×10^{-3}	2.42×10^{-3}
1.6×10^{-3}	12	1.77×10^{-3}	1.73×10^{-3}	1.66×10^{-3}
2.7×10^{-3}	12	1.30×10^{-3}	1.24×10^{-3}	1.16×10^{-3}

Table 3. Variation of F_2 with $\mu_0^2 = Q^2 + m_b^2 + (P_{t_b} + P_{t_{\bar{b}}})^2/4$ for various x and Q^2 values.

Table 4

x	Q^2	$\mu = \mu_0/2$	$\mu = \mu_0$	$\mu = 2\mu_0$
8.5×10^{-4}	8.5	5.34×10^{-5}	4.99×10^{-5}	4.52×10^{-5}
8.5×10^{-4}	12	1.09×10^{-4}	1.04×10^{-4}	1.00×10^{-4}
8.5×10^{-4}	25	4.65×10^{-4}	4.59×10^{-4}	4.50×10^{-4}
8.5×10^{-4}	50	1.57×10^{-3}	1.56×10^{-3}	1.56×10^{-3}
4.2×10^{-4}	12	1.44×10^{-4}	1.42×10^{-4}	1.39×10^{-4}
8.5×10^{-4}	12	1.09×10^{-4}	1.04×10^{-4}	1.00×10^{-4}
1.6×10^{-3}	12	8.21×10^{-5}	7.62×10^{-5}	7.08×10^{-5}
2.7×10^{-3}	12	6.30×10^{-5}	5.67×10^{-5}	5.13×10^{-5}

Table 4. Variation of F_L with $\mu^2 = Q^2 + m_b^2 + (P_{t_b} + P_{t_{\bar{b}}})^2/4$ for various x and Q^2 values.

Figure Captions

Fig.1. The distributions $dF_2(x, Q^2, m_c^2, M)/dM$ for charm production at fixed $x = 8.5\times10^{-4}$ and $Q^2 = 8.5$ (solid line), 12 (dotted line), 25 (short dashed line), 50 (long dashed line) all in units of $(\mathrm{GeV/c})^2$. Histograms are complete $\mathcal{O}(\alpha_s^2)$ result. For comparison we show the Born result times a multiplicative factor of 1.3 (empty box), 1.3 (solid box), 1.2 (empty circle), 1.2 (solid circle) for the various Q^2 values, respectively.

Fig.2. The distributions $dF_L(x, Q^2, m_c^2, M)/dM$ for charm production at fixed $x = 8.5\times10^{-4}$ while varying Q^2. Notation is that of Figure 1 for the $\mathcal{O}(\alpha_s^2)$ result. For comparison we show the Born result times a multiplicative factor of 1.9 (empty box), 1.9 (solid box), 1.6 (empty circle), 1.6 (solid circle) for the various Q^2 values, respectively.

Fig.3 The distributions $dF_2(x, Q^2, m_c^2, M)/dM$ for charm production at fixed $Q^2 = 12\,(\mathrm{GeV/c})^2$ with $x = 4.2\times10^{-4}$ (solid line), 8.5×10^{-4} (dotted line), 1.6×10^{-3} (short dashed line), 2.7×10^{-3} (long dashed line). For comparison we show the Born result times a multiplicative factor of 1.3 (empty box), 1.3 (solid box), 1.3 (empty circle), 1.4 (solid circle) for the various x values, respectively.

Fig.4 The distributions $dF_L(x, Q^2, m_c^2, M)/dM$ for charm production at fixed $Q^2 = 12\,(\mathrm{GeV/c})^2$ while varying x. Notation is that of Figure 3 for the $\mathcal{O}(\alpha_s^2)$ result. For comparison we show the Born result times a multiplicative factor of 1.9 (empty box), 1.9 (solid box), 1.9 (empty circle), 1.5 (solid circle) for the various x values, respectively.

Fig.5. The distributions $dF_2(x, Q^2, m_b^2, M)/dM$ for bottom production at fixed $x = 8.5\times10^{-4}$ while varying Q^2. Notation is that of Figure 1 for the $\mathcal{O}(\alpha_s^2)$ result but all points are 1.3× Born result for the various Q^2 values, respectively.

Fig.6. The distributions $dF_L(x, Q^2, m_b^2, M)/dM$ for bottom production at fixed $x = 8.5\times10^{-4}$ while varying Q^2. Notation is that of Figure 1 for the $\mathcal{O}(\alpha_s^2)$ result but all points are 1.3× Born result for the various Q^2 values, respectively.

Fig.7 The distributions $dF_2(x, Q^2, m_b^2, M)/dM$ for bottom production while varying x at fixed $Q^2 = 12\,(\mathrm{GeV/c})^2$. Notation is that of Figure 2 for the $\mathcal{O}(\alpha_s^2)$ result but all points are 1.3× Born result for the various x values, respectively.

Fig.8 The distributions $dF_L(x, Q^2, m_b^2, M)/dM$ for bottom production while varying x at fixed $Q^2 = 12\,(\mathrm{GeV/c})^2$. Notation is that of Figure 2 for the $\mathcal{O}(\alpha_s^2)$ result but all points are 1.3× Born result for the various x values, respectively.

References

[1] E. Laenen, S. Riemersma, J. Smith and W. L. van Neerven, Nucl. Phys. **B392** (1993) 162.

[2] E. Laenen, S. Riemersma, J. Smith and W. L. van Neerven, Nucl. Phys. **B392** (1993) 229.

[3] S. Riemersma, J. Smith and W. L. van Neerven, Rates for Inclusive Deep-Inelastic Electroproduction of Charm Quarks at HERA, SMU-HEP 94-25, to appear in Physics Letters B.

[4] H. L. Lai, J. Botts, J. Huston, J. G. Morfín, J. F. Owens, J. W. Qiu, W. K. Tung and H. Weerts, MSU-HEP-41024 (Oct. 1994).

[5] H1 Collaboration, I. Abt, et al., Nucl. Phys. **B407** (1993) 515; ZEUS Collaboration, M. Derrick et al., Phys. Lett. **B316** (1993) 412.

[6] R.K. Ellis and P. Nason, Nucl. Phys. **B312** (1989) 551; S. Frixione, M. L. Mangano, P. Nason and G. Ridolfi, CERN-TH 7527/94.

[7] J. Smith and W. L. van Neerven, Nucl. Phys. **B374** (1992) 36; W. L. van Neerven, Nucl. Phys. **B29A** (Proc. Suppl.) (1992) 199.

[8] S. Frixione, M. L. Mangano, P. Nason, and G. Ridolfi, Nucl. Phys. **B412** (1994) 225; M. L. Mangano, P. Nason, and G. Ridolfi, Nucl. Phys. **B373** (1992) 295.

[9] G. A. Schuler, Nucl. Phys. **B299** (1988) 21; A. Ali, G. Ingelman, G.A. Schuler, F. Barreiro, M.A. García, J.F. de Trocóniz, R.A. Eichler and Z. Kunszt, Heavy quark physics at HERA, Proc. DESY workshop on HERA physics, DESY, Hamburg(1988), DESY 88-119; A. Ali and D. Wyler in Physics at HERA, vol 2 p. 669, Proceedings of the Workshop Hamberg, Oct 29 (1991) Eds. W. Buchmüller and G. Ingelman; A. Ali, DESY 93-105.

[10] J. C. Collins, D. E. Soper, and G. Sterman in *Perturbative QCD* ed. A. H. Mueller (World Scientific, 1989).

[11] B. W. Harris and J. Smith, in preparation.

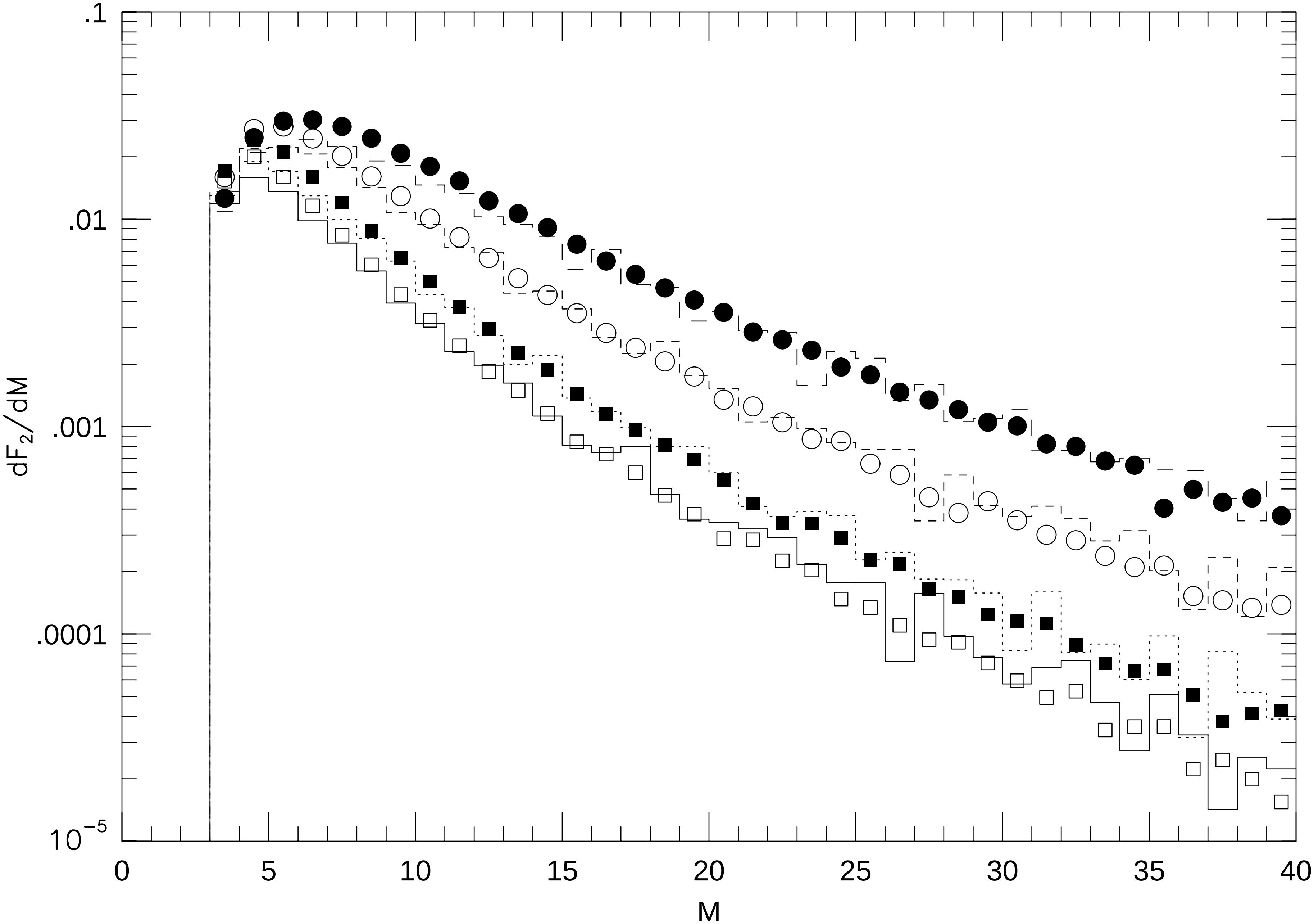
.1
.01
.001
.0001
10^{-5}
0
5
10
15
20
25
30
35
40
M
dF_2/dM

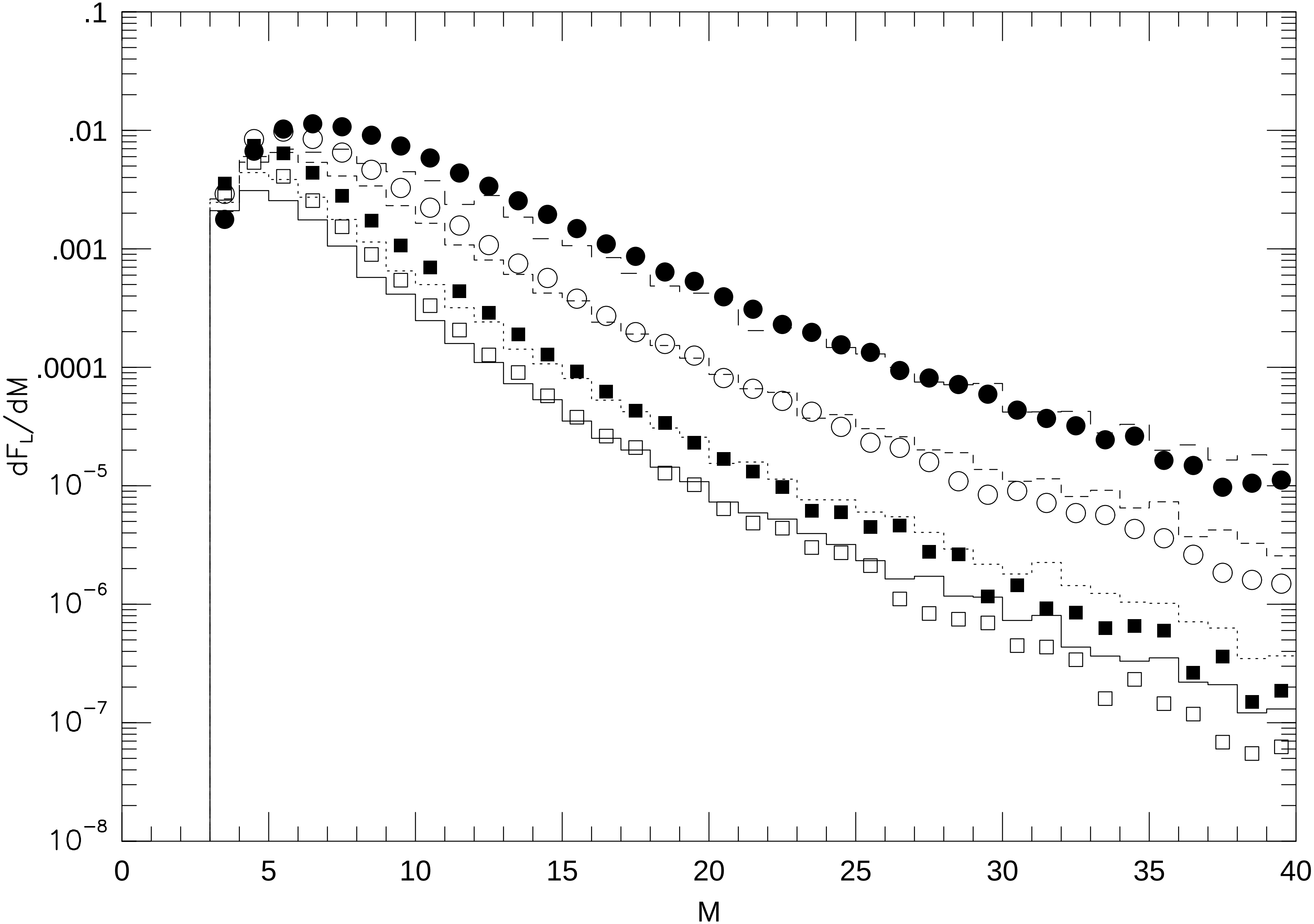

.1
.01
.001
.0001
10^{-5}
10^{-6}
10^{-7}
10^{-8}
dF_L/dM
0
5
10
15
20
25
30
35
40
M

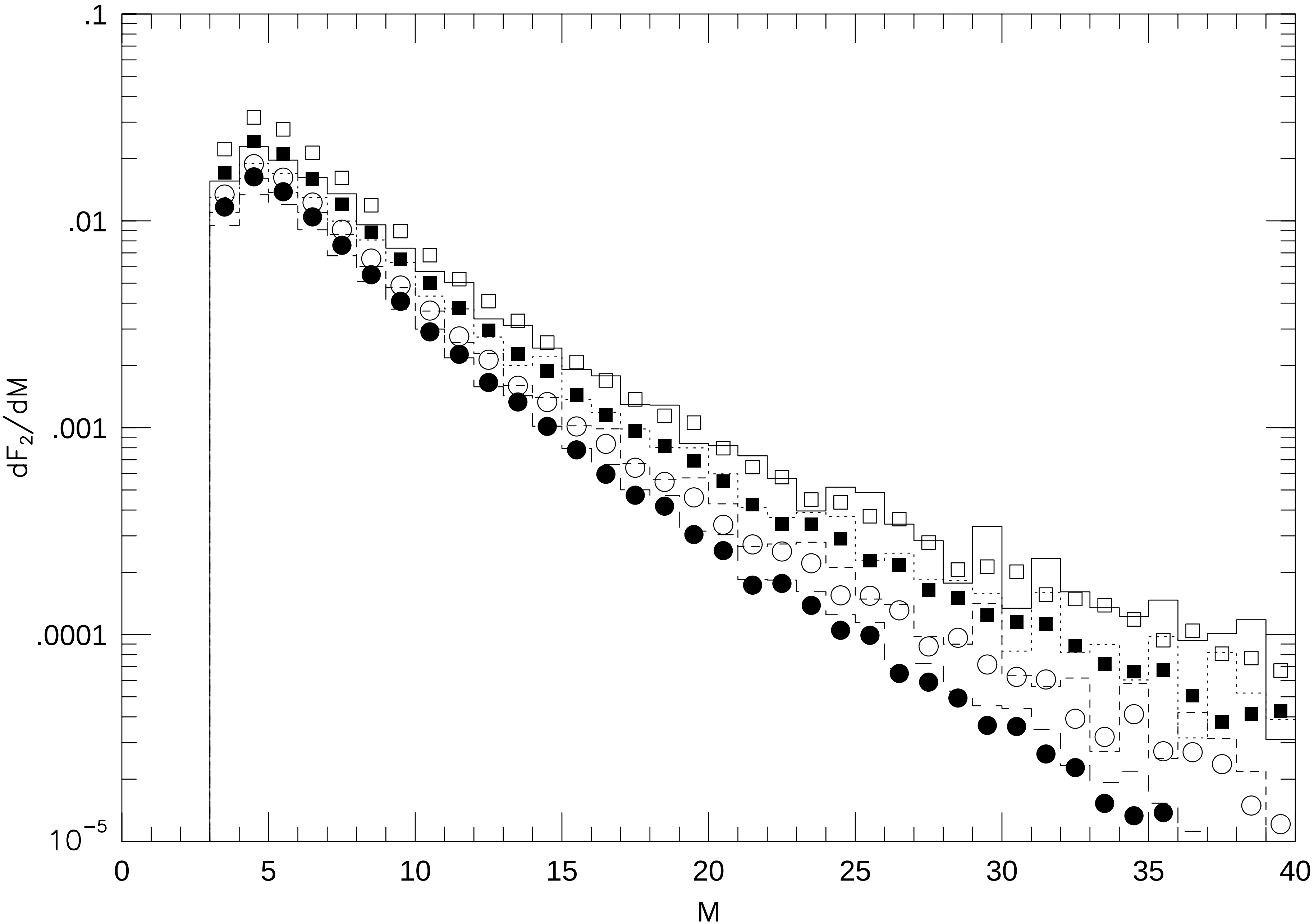

.1
.01
.001
.0001
10^{-5}
0
5
10
15
20
25
30
35
40
M
dF_2/dM

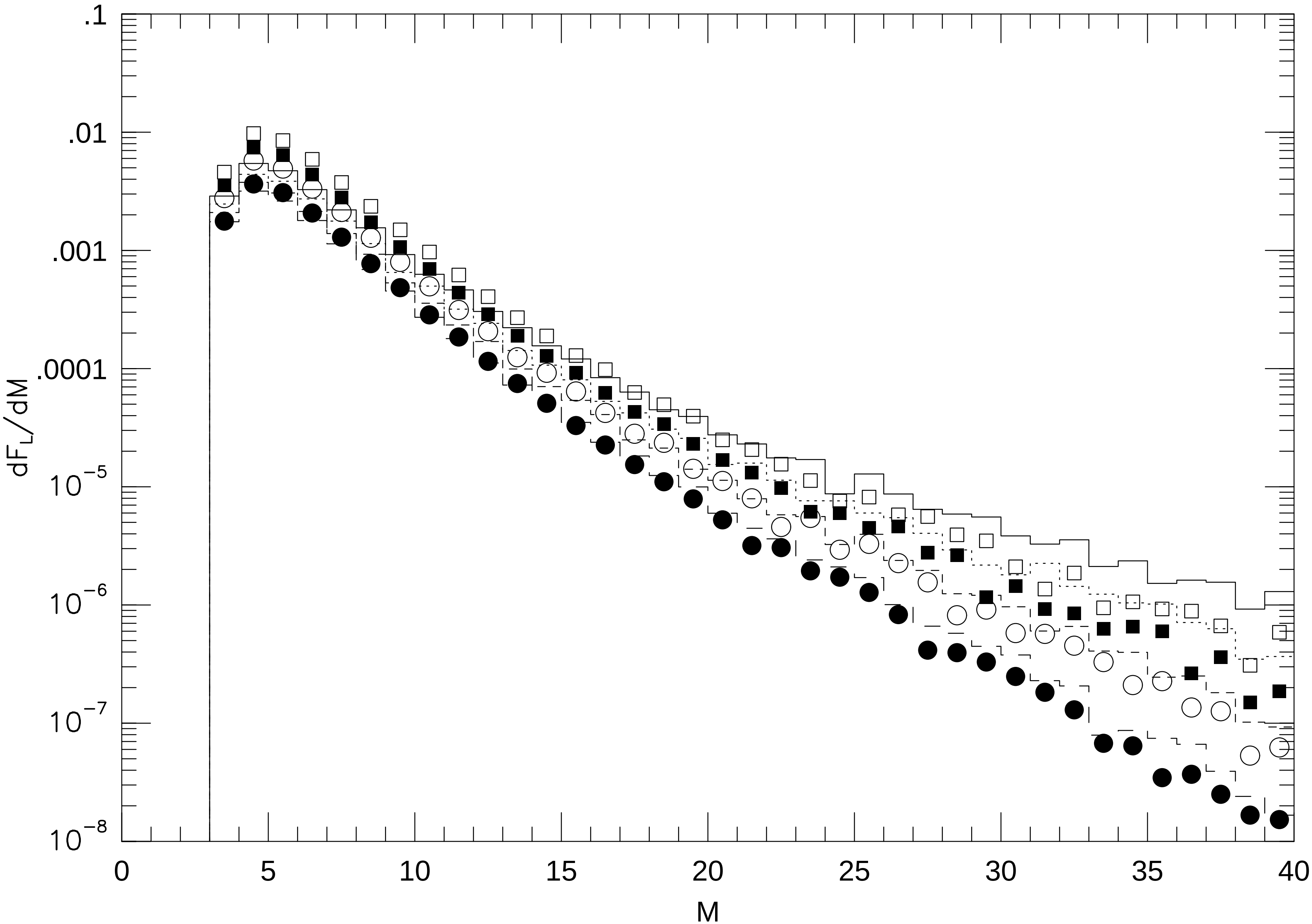

.1
.01
.001
.0001
10^{-5}
10^{-6}
10^{-7}
10^{-8}
dF_L/dM
0
5
10
15
20
25
30
35
40
M

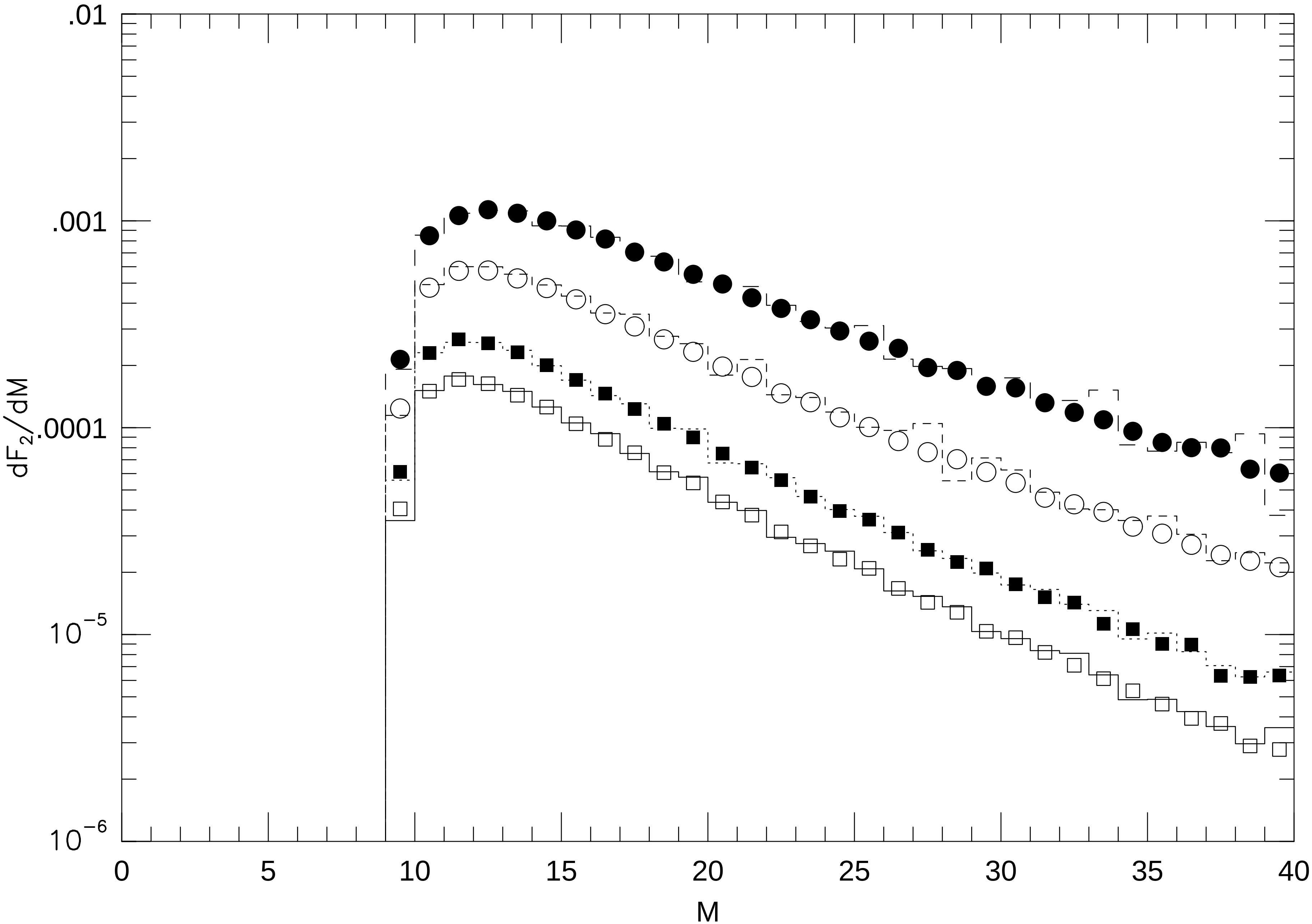

.01
.001
.0001
10^{-5}
10^{-6}
0
5
10
15
20
25
30
35
40
M
dF_2/dM

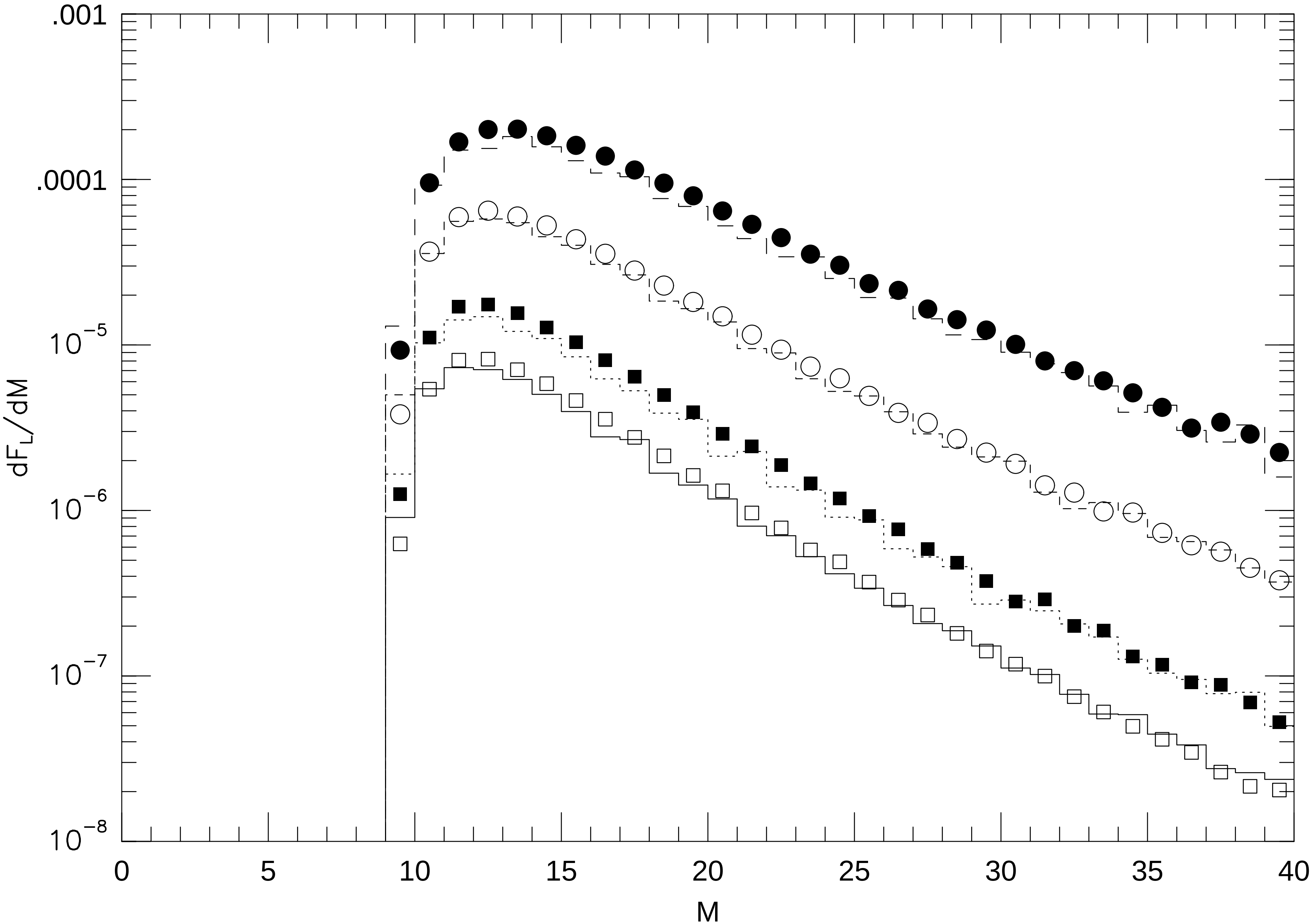
.001
.0001
10^{-5}
10^{-6}
10^{-7}
10^{-8}
dF_L/dM
0
5
10
15
20
25
30
35
40
M

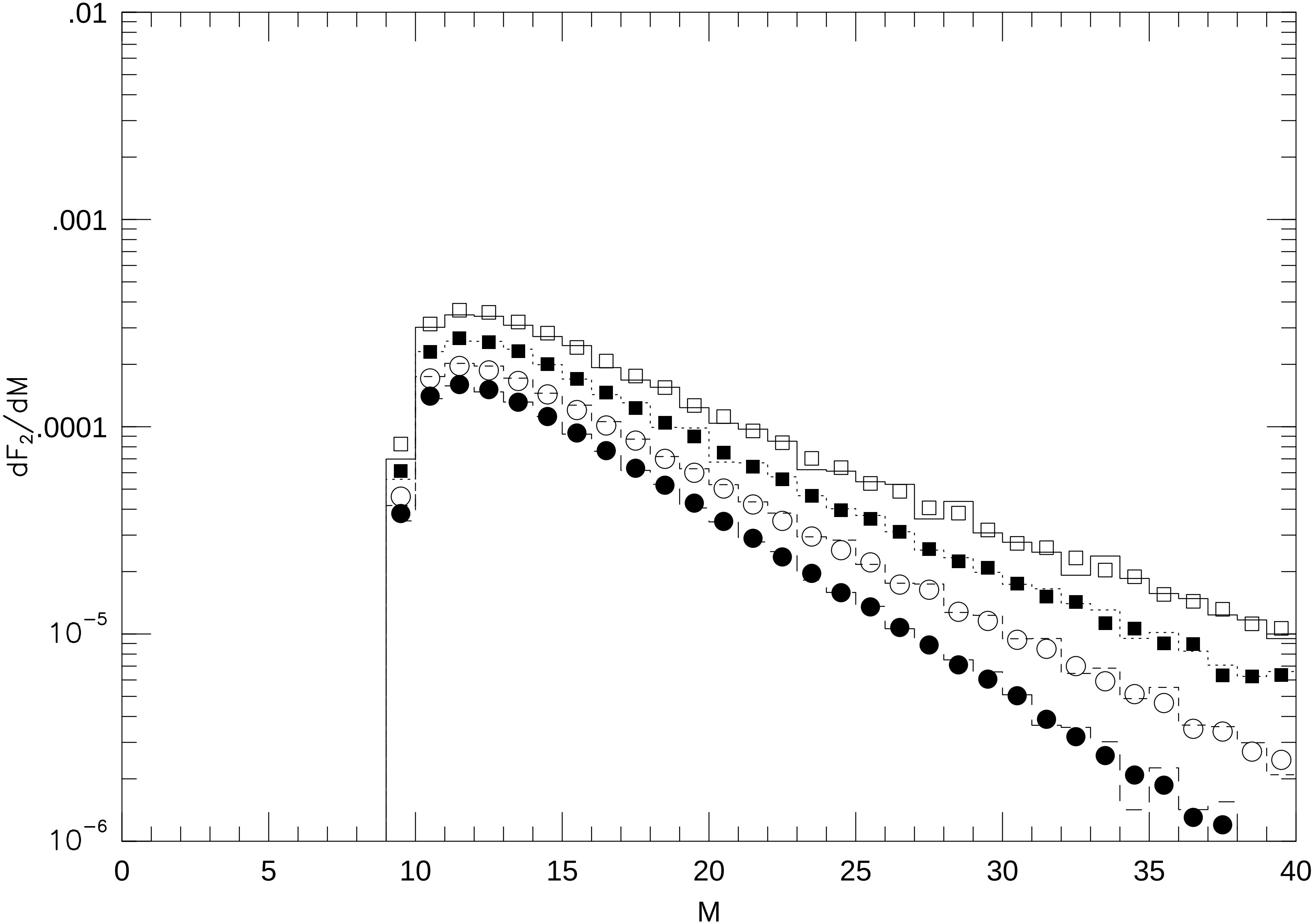

.01
.001
.0001
10^{-5}
10^{-6}
dF_2/dM
0
5
10
15
20
25
30
35
40
M

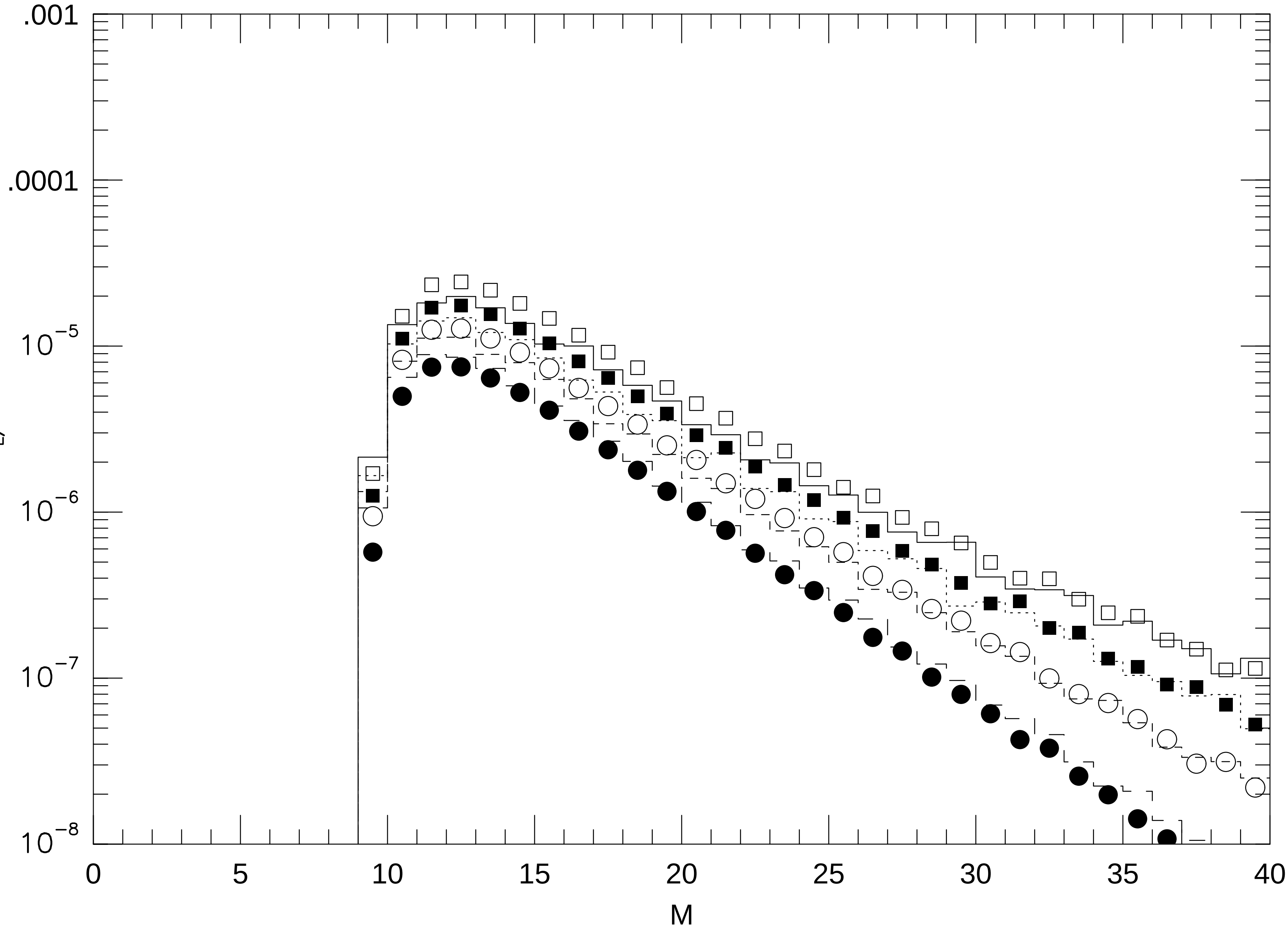
.001
.0001
10^{-5}
10^{-6}
10^{-7}
10^{-8}
dF_L/dM
0
5
10
15
20
25
30
35
40
M